DRAFT VERSION NOVEMBER 13, 2008
Preprint typeset using LaTeX style emulateapj v. 10/09/06

arXiv:0811.2014v1 [astro-ph] 13 Nov 2008

PREDICTIONS OF QUASAR CLUSTERING: REDSHIFT, LUMINOSITY AND SELECTION DEPENDENCE

ROBERT J. THACKER[1,2], EVAN SCANNAPIECO[3], H. M. P. COUCHMAN[4] AND MARK RICHARDSON[1]

Draft version November 13, 2008

ABSTRACT

We show that current clustering observations of quasars and luminous AGN can be explained by a merger model augmented by feedback from outflows. Using numerical simulations large enough to study clustering out to 25 comoving h^{-1} Mpc, we calculate correlation functions, biases, and correlation lengths as a function of AGN redshift and optical and X-ray luminosity. At optical wavelengths, our results match a wide range of current observations and generate predictions for future data sets. We reproduce the weak luminosity dependence of clustering over the currently well-measured range, and predict a much stronger dependence at higher luminosities. The increase in the amplitude of binary quasar clustering observed in the Sloan Digital Sky Survey (SDSS) is also reproduced and is predicted to occur at higher redshift, an effect that is due to the one halo term in the correlation function. On the other hand, our results do not match the rapid evolution of the correlation length observed in the SDSS at $z \simeq 3$, a discrepancy that is at least partially due to differences in the scales probed by our simulation versus this survey. In fact, we show that changing the distances sampled from our simulations can produce changes as large as 40% in the fitted correlation lengths. Finally, in the X-ray, our simulations produce correlation lengths similar to that observed in the *Chandra* Deep Field (CDF) North, but not the significantly larger correlation length observed in the CDF South.

Subject headings: quasars: general – quasars: clustering – galaxies: evolution

1. INTRODUCTION

Despite numerous observational efforts, quasar clustering and its dependency on luminosity remains controversial. Early studies suggesting that clustering decreases with redshift (Iovino & Shaver 1988; Croom & Shanks 1996) are opposed by more recent observations, which suggest a more complicated clustering history that gradually increases with redshift (Kundic 1997; La Franca *et al.* 1998; Porcani *et al.* 2004; Croom *et al.* 2005). In particular, $z < 2$ studies with the Sloan Digital Sky Survey (SDSS, Myers *et al.* 2006, 2007a, 2007b) and 2QZ (Croom *et al.* 2005, Porcani & Norberg 2006) have uncovered weak evidence for clustering evolution, while above $z = 2$ the SDSS indicates strong evolution in clustering (Shen *et al.* 2007) and 2QZ shows a somewhat weaker increase (Croom *et al.* 2005). Over all these redshifts, the luminosity dependence of clustering is weak (Porciani *et al.* 2004; Adelberger & Steidel 2005; Croom *et al.* 2005; Myers 2006, 2007a), which is usually interpreted as being problematic for quasar models in which AGN luminosity is correlated with proxies for halo mass.

While questions of obscuration and completeness surround optical selection techniques, hard X-ray observations are largely unaffected by obscuration, thus making them perhaps the best candidate for identifying AGNs (Mushotsky 2004). At redshifts $z < 1$ considerable effort has been put into measuring X-ray selected AGNs in both hard (2-10 keV) and soft (0.5-2 keV) bands (*e.g.* Mullis *et al.* 2004; Gilli *et al.* 2005; Basilakos *et al.* 2004, 2005; Yang *et al.* 2006; Miyaji *et al.* 2007). While optical $z < 1$ surveys tend to produce correlations lengths between 5-6 h^{-1} Mpc (e.g. Porciani & Nordberg 2006), X-ray selected catalogs at these redshifts give correlation lengths in the range 7-8 h^{-1} Mpc (*e.g.* Mullis *et al.* 2004). However, the X-ray selected AGN from the *Chandra* Deep Field-North and South (CDF-N and CDF-S), exhibit significant variances in both the correlation length and power-law slope fits. Thus, Gilli *et al.* (2005), using the full catalog from 0.5-8 keV, found a correlation length of 5.5 ± 0.6 h^{-1} Mpc for the CDF-N, in agreement with optical surveys, and 10.3 ± 1.7 h^{-1} Mpc for the CDF-S, which is clearly in disagreement. This is surprising given that the $\log N - \log S$ of the two fields agree well. A recent re-analysis of this data, binned by luminosity and separating into hard and soft classifications, has yielded essentially the same overall result (Plionis *et al.* 2008), but elucidated that the two fields have much more consistent clustering behavior when binned by luminosity. Previous analyses had suggested the difference in clustering could be attributed solely to sample variance due to the lack of large superclusters in the CDF-S (Gilli *et al.* 2003).

While AGN/quasar feedback has become theoretically favored as a necessary component of galaxy evolution (*e.g.* Scannapieco & Oh 2004, hereafter SO04; Granato *et al.* 2004; Croton *et al.* 2006), direct observational evidence of this idea remains somewhat weak. The paucity of high-redshift X-ray objects also makes studying clustering evolution of X-ray catalogs difficult. However, Francke *et al.* (2008) have cross-correlated AGN from the Extended CDF-S and luminous blue galaxy sources at $z \approx 3$ identified in the MUSYC survey (Gawiser *et al.* 2006). Their results indicate that the AGN targeted in the survey are more clustered than star-forming luminous blue galaxies, a result consistent with the idea that typical AGNs tend to sit in more massive halos than the average galaxy population. Clearly there remain many open questions about the clustering properties of optical and X-ray selected AGN, and the ongoing CDF controversy suggests that we can learn a great deal by comparing to predictions of clustering from simulations.

From a theoretical perspective, early models of quasar formation associated quasars with galaxy mergers and assumed a close relationship between black hole mass and luminos-

[1] Department of Astronomy and Physics, Saint Mary's University, Halifax, Nova Scotia, B3H 3C3, Canada.
[2] Canada Research Chair
[3] School of Earth and Space Exploration, Arizona State University, PO Box 871404, Tempe, AZ, 85287-1404.
[4] Department of Physics and Astronomy, McMaster University, 1280 Main St. West, Hamilton, Ontario, L8S 4M1, Canada.

ity (*e.g.* Kauffmann & Haehnelt 2000; Wyithe & Loeb 2002, 2003). In this case, the black hole mass was calculated either by using the $M_{\rm BH}-\sigma$ relationship (Ferrarese & Merrit 2000) or associating $M_{\rm BH}$ with the halo circular velocity (Merrit & Ferrarese 2001; Tremaine *et al.* 2002; Ferrarese 2002). Such "light bulb" models successfully match the luminosity function of high-redshift quasars (*e.g.* Wyithe & Loeb 2003), but become progressively more inaccurate at low redshifts when feedback processes become important (*e.g.* SO04). Cosmological simulations using the $M_{\rm BH}-\sigma$ framework and incorporating feedback have managed to reproduce the turn-down in the quasar luminosity function with moderate success (Thacker *et al.* 2006, hereafter TSC06). However, there appear to be differences between the detailed behavior of gas in simulations versus semi-analytic models, which are primarily due to differences between shock-heating in a uniform medium relative to an inhomogeneous one (*e.g.* Helley *et al.* 2003; Nagamine *et al.* 2005; Croton *et al.* 2006; Cattaneo *et al.* 2006; Cattaneo *et al.* 2007; Di Matteo *et al.* 2008).

More recent models (*e.g.* Hopkins *et al.* 2005a, 2005b, 2005c, 2006a, 2006b, 2007a), motivated by numerical modeling of black hole accretion during mergers (Di Matteo *et al.* 2005; Springel *et al.* 2005a, 2005b; Robertson *et al.* 2006a, 2006b; Cox *et al.* 2006a, 2006b), suggest that quasar activity is comparatively decoupled from galaxy mass. This picture entails complex relationships between a distinct sequence of AGN evolutionary epochs and the feedback processes that regulate them (*e.g.* Hopkins *et al.* 2007a). The resulting behavior is one in which the bright end of the luminosity function corresponds to quasars radiating at close to their peak luminosities near the Eddington limit, while the faint end corresponds to the same population radiating in the faint part of their light curve, at or below ≈ 0.1 of the Eddington luminosity (Hopkins *et al.* 2005b). As a result, clustering is only a weak function of luminosity (Lidz *et al.* 2006). While the exact dynamics of nuclear accretion flows are still beyond the resolution of simulations of colliding galaxies, and are still the subject of much active research and modeling (*e.g.* Proga *et al.* 2008), the overall phenomenology in this model of quasar activity is well understood. Recent increases in computing capacity have lead to simulations of this model in a cosmological environment and investigations of the impact of AGN on disk formation (*e.g.* Sijacki *et al.* 2007; Di Matteo *et al.* 2008; Okamoto *et al.* 2008).

In our earlier work (TSC06) we incorporated the merger and feedback AGN model of SO04 into a large cosmological smooth particle hydrodynamic simulation. However, our analysis of the clustering properties of optically-selected AGNs was constrained to a single luminosity bin and did not consider redshift evolution in any significant depth. In view of several recent ground-based surveys, it is therefore timely to reanalyze our simulation to address both the luminosity dependence and redshift evolution of clustering. Furthermore, the advent of new X-ray selected AGN catalogs with optical follow-up also allows us to present an analysis of the clustering of an X-ray selected catalog.

We stress that the aim of this paper is not to encourage support for one quasar model over another, but rather to examine whether the details of the faint part of the light curve are actually needed to accurately predict currently observed clustering statistics. Since the SO04 model does not include a low luminosity accretion period we can indirectly constrain the importance of this epoch to quasar clustering behavior. This should not be interpreted as constraining whether such a period does actually occur, or for that matter, the relative length of such a period.

The layout of the paper is as follows: in §2 we give a summary of our simulations and overall method. In §3 we present a detailed analysis of clustering at $z = 1.5$, 2.0, and 3.0 and the dependence of this clustering on luminosity. In §4 we examine the clustering properties of X-ray selected AGN, again as a function of redshift and luminosity. We close with a brief discussion in §5. Throughout the paper we consider a pre-WMAP3 (Spergel *et al.* 2003) ΛCDM model with parameters $h = 0.7$, $\Omega_0 = 0.3$, $\Omega_\Lambda = 0.7$, $\Omega_b = 0.046$, $\sigma_8 = 0.9$, and $n = 1$, where h is the Hubble constant in units of 100 km s^{-1} Mpc^{-1}, Ω_0, Ω_Λ, and Ω_b are the total matter, vacuum, and baryonic densities in units of the critical density, σ_8^2 is the variance of linear fluctuations on the $8h^{-1}$Mpc scale, and n is the "tilt" of the primordial power spectrum. While we consider only a fixed σ_8 in our simulation, the overall impact of changing σ_8 on fitted correlation functions ($\xi(r) = (r_0/r)^\gamma$) is to change the correlation length r_0. For correlation functions with $\gamma \approx 2$, increasing σ_8 by a factor of f will increase the correlation length of unbiased tracers of mass by the same factor. Throughout the paper the Eisenstein & Hu (1999) transfer function is used and we quote all distances in comoving coordinates.

2. SIMULATION METHOD AND QUASAR MODELING

We consider two simulations in this study. The first is a "fiducial" run containing star formation and our model of AGN outflows (TSC06) in a periodic cube 146 h^{-1} Mpc on a side, containing 2×640^3 particles. With these choices the dark-matter particle mass is $1.9 \times 10^8 M_\odot$ and the gas particle mass is $2.7 \times 10^7 M_\odot$. The second simulation, which we call the "comparison" run, uses 2×320^3 particles in a periodic cube of size 73 h^{-1} Mpc, which matches the particle mass in the fiducial run, and includes star formation but not AGN outflows (Scannapieco *et al.* 2008). Both simulations were conducted with a parallel OpenMP based implementation of the "HYDRA" code (Thacker & Couchman 2006) that uses the Adaptive Particle-Particle, Particle-Mesh algorithm to calculate gravitational forces (Couchman 1991), and the smooth particle hydrodynamic method to calculate gas forces (Lucy 1977; Gingold & Monaghan 1977). Due to computational cost as well as the limitations of our modeling, both simulations were halted at $z = 1.2$.

Our method, as outlined in TSC06, associates quasar-phase AGN with galaxy mergers, which are tracked within the simulations by identifying gas groups and applying group number labels to their particles. Mergers are groups for which at least 30% of the accreted mass does not come from a single massive progenitor, and we calculate the mass of the associated black hole, $M_{\rm BH}$, using the circular velocity of the new system, $v_{\rm c}$, and the observed $M_{\rm BH}-v_{\rm c}$ relation (Merrit & Ferrarese 2001; Tremaine *et al.* 2002; Ferrarese 2002). We note that observational evidence of the universality of this relationship is still restricted to low redshift systems, and there is modest evidence that the normalization changes somewhat with redshift (*e.g.* Woo *et al.* 2008). Continuing, our modeling approach yields

$$M_{\rm BH} = 2.8 \times 10^8 \left(\frac{v_{\rm c}}{300\,{\rm km\,s^{-1}}}\right)^5, \qquad (1)$$

where $v_{\rm c}$ is estimated from

$$v_{\rm c} = \left[\frac{4\pi}{3} G \rho_{\rm v}(z) r_{\rm v}^2\right]^{1/2}, \qquad (2)$$

and G is the gravitational constant, $\rho_{\rm v}(z)$ is the virial density as a function of redshift, and $r_{\rm v}$ is the implied virial radius for a group of N gas particles with mass $m_{\rm g}$

$$r_{\rm v} = \left[\frac{N m_{\rm g} \Omega_0/\Omega_b}{4/3\pi\rho_{\rm v}(z)}\right]^{1/3}. \quad (3)$$

In keeping with the model outlined in Wyithe & Loeb (2002) and SO04, we assume that for each merger the accreting black hole shines at its Eddington luminosity (1.2×10^{38} ergs s^{-1} $M_\odot{}^{-1}$) for a time taken to be a fixed fraction, 0.055, of the dynamical time of the system, $t_{\rm AGN} = 0.055 r_{\rm v}/v_{\rm c} = 5.8\times10^{-3}\Omega(z)^{-1/2}H(z)^{-1}$. We have shown in earlier work (TSC06) that apart from a small discrepancy at the most luminous end of the luminosity function, these simple assumptions lead to a model that reproduces the observed AGN luminosity function as well as the predictions of SO04. Furthermore, we were able to demonstrate that this discrepancy can be explained in terms of the relative efficiency of shock heating on substructure, and corrected for if necessary by post-processing our simulations, as discussed in further detail below. An initial analysis of clustering properties was also in close agreement with observations, particularly the small-scale, $r \lesssim 1h^{-1}$ Mpc, clustering of quasars (*e.g.* Hennawi *et al.* 2006).

Perhaps the most problematic aspect of this model is that it makes no distinction between AGN formed by gas-rich "wet" mergers versus those formed by gas-poor "dry" mergers. As we implement star formation on the basis of a simple merger model and ignore the quiescent mode of star formation, it is difficult for us to make this distinction with any confidence. However, while there is significant evidence that at low redshifts the quiescent mode of star formation dominates (Noeske *et al.* 2007), at higher redshifts there is good reason to believe that mergers are necessary to fuel observed high star formation rates (*e.g.* Erb 2008). We can also appeal to the fact that while at $z = 0$ dry mergers are important, they will be less so at $z = 1.2$. For example, the semi-analytic estimates presented in Hopkins *et al.* (2007), in particular their Figure 5, show that that the ratio of gas-rich to gas poor $4\times10^{12}M_\odot$ mergers, ranges from 10:1 at $z = 2$, to 2:1 at $z = 1$, indicating that gas-poor mergers are relatively unimportant before our final redshift.

In the calculation of wind velocity we assume that a fixed fraction $\epsilon_{\rm k} = 0.05$ of the bolometric energy of each AGN is channeled into a kinetic outflow, while the remainder is emitted as light. While there is much debate about variability of this value on a system-by-system basis, our choice is consistent with other literature estimates (*e.g.* Furlanetto & Loeb 2001; Nath & Roychowdhury 2002), as well as observations (Chartas *et al.* 2007). If we restrict ourselves to the consideration of systems with large bulges, then the resulting level of kinetic energy input is considerably greater than that from supernovae and stellar winds (*e.g.* Kravtsov & Yepes 2000; Tozzi *et al.* 2000; Brighenti & Mathews 2001; Babul *et al.* 2002; Tornatore *et al.* 2004). Using the Eddington luminosity, associated dynamical time and the wind efficiency, each AGN outflow is launched with a wind energy of

$$E_{\rm k} = 6\times10^{36}\left(\frac{M_{\rm bh}}{\rm M_\odot}\right)\left(\frac{t_{\rm d}}{\rm s}\right)\ {\rm ergs}. \quad (4)$$

Since there are considerable uncertainties about the precise geometry of AGN outflows, we have chosen to use a spherical shell to represent the outflow. Even strongly bipolar systems will tend to release an ellipsoidal cocoon of gas (*e.g.* Begelman & Cioffi 1989; Yamada *et al.* 1999), so this approximation is reasonable. We thus model each expanding outflow as a spherical shell at a radius $2r_{\rm v}$ which is created by rearranging the gas between $r_{\rm v}$ and $2r_{\rm v}$ which lies below a density threshold of $2.5\rho_{\rm v}$. In Figure 1 we present a plot of local gas density in a 12 h^{-1} Mpc region with the position of the virial and launching radii indicated. The radial velocity of the shell v_s is set by ensuring that the sum of the thermal and kinetic wind energies is equal to $E_{\rm k} - E_{\rm grav}$ where $E_{\rm grav}$ is the potential energy change required to move the particles to $2r_{\rm v}$. The post-shock temperature of the wind is given by

$$T_s = 13.6\,{\rm K}\left(\frac{v_s}{\rm km\,s^{-1}}\right)^2. \quad (5)$$

This model produces a level of preheating in galaxy clusters and groups that is in good agreement with observations as discussed in TSC06, to which the reader is referred for further details about our simulations.

3. OPTICALLY-SELECTED AGN

3.1. *Optical Quasar Luminosity Function Revisited*

As a test of our overall approach, our first step is to repeat the optical luminosity function analysis of TSC06, but for both simulations and for ranges of redshifts binned so as to make them most useful for comparisons with clustering measurements. As previously, we construct the luminosity function by binning in luminosity and redshift. We calculate the number of quasars in each bin times the total time these objects are shining, and divide by the time interval, the width of the bin, and the volume of the simulation. That is for a given redshift bin i and a given luminosity bin j the luminosity function is simply

$$\Psi_{i,j} = \frac{1}{V\Delta t_i \Delta L_{B,j}} \sum_{k\in{\rm bin_{i,j}}} t_{{\rm AGN},k}, \quad (6)$$

where the sum is over the lifetimes of all quasars with redshifts and luminosities associated with the i, j bin, which spans a time interval Δt_i and a range of luminosities $\Delta L_{B,j}$. The resulting luminosity functions for the fiducial AGN-feedback run and the comparison run are shown in Figure 2, in which the error bars are 1-sigma estimates, computed as $\Delta\Psi_{i,j} = \Psi_{i,j}[1\pm(1+N_{i,j})^{-1/2}]$, where $N_{i,j}$ is the number of quasars contributing to bin i,j. As discussed in TSCO6, our fiducial model shows a clear turn-down in the number of $L_B \geq 10^{13}$ quasars at $z < 2$, which parallels the observational trend, but still overestimates the number of luminous and low-redshift quasars due to numerical effects. Likewise, the luminosity function in the no-feedback simulation continues to rise at low redshift, increasing along with the halo merger rate as discussed in Wyithe & Loeb (2003). Thus, this simple model fails to reproduce the drop in the number density of $z \leq 2$ quasars as discussed in SO04 and Scannapieco *et al.* (2008).

Finally, we include a luminosity function calculated to match the shock behavior in the semi-analytic SO04 model. This was achieved by removing neighboring objects from the simulation that are found inside a shock radius calculated using the SO04 model (see TSC06 for an extended discussion of this analysis). After we apply this algorithm, the simulation results much more closely match the observations.

3.2. *Dependence of the Correlation Function on Redshift and Luminosity*

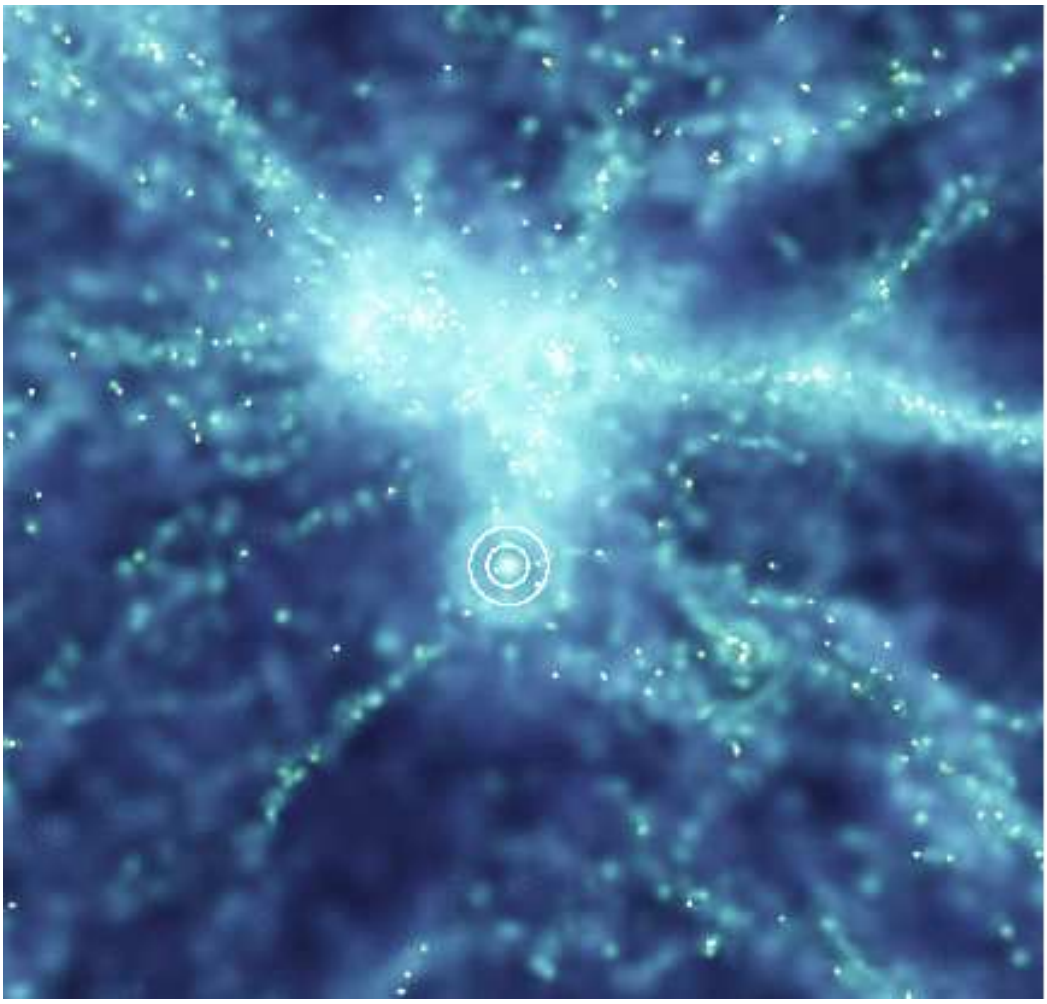

FIG. 1.— Schematic representation of the impact of outflows on the local density of gas. The region shown is 12 h^{-1} Mpc across (comoving), at a redshift of z=1.59. The the virial radius, r_v, of a system with a baryonic mass of $6 \times 10^{10}\,M_{\odot}$ is represented by the inner circle, the outer circle corresponds to $2r_v$, denoting the launching point of an outflow for this system. A number of outflow events with different characteristic radii are visible within this small volume.

Having outlined the successes and limitations of our model in reproducing the observed number density of quasars, we next move on to a detailed study of their spatial distribution. Here our primary tool is the real-space auto-correlation function, calculated as

$$\xi_{\rm qq}(r,z,L)+1 = \frac{DD(r,z,L)}{RR(r,z,L)}, \qquad (7)$$

where $DD(r,z,L)$ is the number of pairs at a given comoving distance within a given redshift bin and with a luminosity within a given interval, and $RR(r,z,L)$ is the average number of such pairs that would be found at this separation in a random distribution. Here we have correlated all quasars within each redshift bin, regardless of whether the two objects are shining simultaneously. While this vastly improves the statistical signal, the use of a relatively large redshift window places a lower limit on the spatial scales that we can study, because the peculiar motions can shift the positions of the quasars during the finite time window associated with each bin. For our choices of redshift intervals, and estimating typical peculiar velocities of quasars at ≈ 300 km/s, this places a lower limit of 0.5 h^{-1} Mpc. Note that intrinsic velocity dispersion is estimated from the properties of the halos in which the majority of quasars are contained, and is somewhat smaller than observed pairwise dispersions (*e.g.* da Angela *et al.* 2005), which include both intrinsic and observational errors.

The finite volume of our simulation places an upper limit on the distance we can study of approximately 1/5 the box size (Scoccimarro 1998; Szapudi *et al.* 1999), which corresponds to 30 h^{-1} Mpc in the AGN feedback run and 15 h^{-1} Mpc in the comparison run. To be especially conservative we use a cutoff radius of $10h^{-1}$ Mpc for most of our results, which allows a direct comparison of the fiducial and comparison runs. For the fiducial run alone we also examine the impact of changing to a $25h^{-1}$ Mpc cutoff. In each bin the error bars have be computed using a simple 1-sigma Poisson estimate of $\Delta\xi_{\rm qq}(r,z,L) = \xi_{\rm qq}(r,z,L)[1 \pm (1+DD(r,z,L))^{-1/2}]$

With these limitations in mind, in Figure 3 we plot the correlation function of simulated quasars, dividing our sample into three luminosity bins from $L_B = 10^{11} - 10^{12} L_{\odot,B}$, $L_B = 10^{12} - 10^{13} L_{\odot,B}$, and $L_B = 10^{13} - 10^{14} L_{\odot,B}$. Focusing first on the AGN feedback run, the most striking feature of this plot is the relative lack of clustering at large separations and low redshifts, which occurs even though our model assumes accretion at the Eddington rate for all active black holes. Perhaps contrary to initial expectations, this weak dependence blankets the range of redshifts and separations that are best constrained observationally, suggesting that complex accretion histories may not play a key role in explaining current optical measurements.

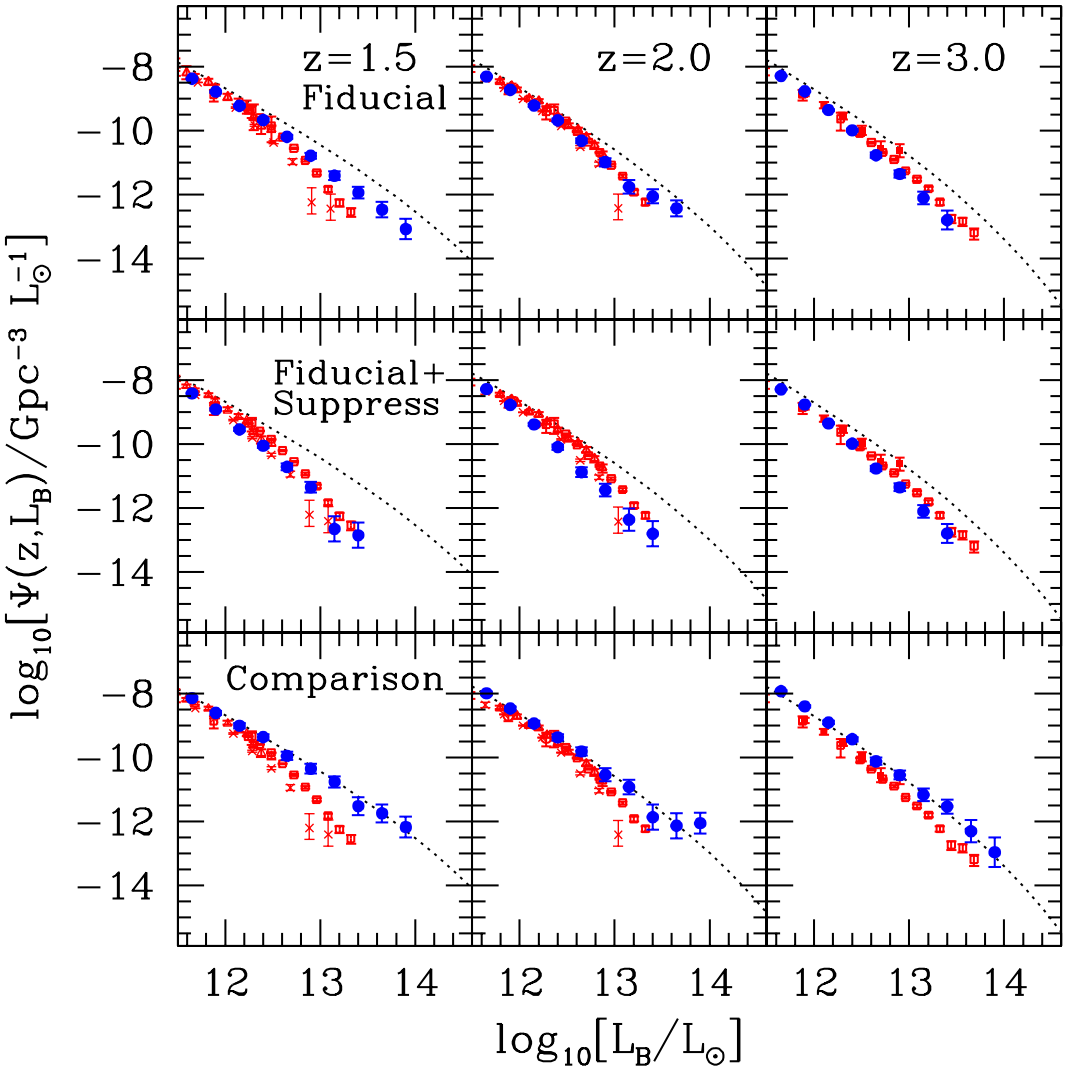

FIG. 2.— Evolution of the B-band quasar luminosity function. The simulation results are given by the solid circles, while the dotted line is the simple estimate from the analytic model of Wyithe & Loeb (2003). From left to right the columns give results at redshifts of $1.2-1.75$, $1.75-2.25$, and $2.25-4.0$. From top to bottom, the rows show results from the fiducial run, the fiducial run with additional suppression imposed (by removing neighboring systems below a heating threshold), and the comparison run. In all panels error bars are 1-sigma Poisson estimates. The observational data are taken from Croom *et al.* (2004, crosses) Richards *et al.* (2005, open triangles), Richards *et al.* (2006, open squares), Wolf *et al.* (2003, open circles), and Siana *et al.* (2008, filled squares).

Note, however, that very different behavior occurs both at the smallest separations and at the highest redshifts, with ξ_{qq} showing a strong luminosity dependence in both these regimes. Each of these enhancements is likely to be caused by different processes. At small separations, the strong dependence is likely to be a manifestation of so-called "one-halo effects" (*e.g.* Berlind & Weinberg 2002; Bullock *et al.* 2002; van den Bosch *et al.* 2003; Magliocchetti & Porciani 2003) which take place when gravitationally-bound objects orbit each other within the same potential, adding significantly to the correlation function at distances smaller than the virial radius. This small-scale upturn, which has been confirmed observationally for SDSS quasars (Hennawi *et al.* 2006; Serber *et al.* 2006; Myers *et al.* 2007b), occurs at the radius corresponding to the maximum apocenter of such gravitationally-bound pairs, which in turn corresponds to the virial radius of the halos in which they are contained. As the most luminous AGN live in the deepest gravitational potential wells in our model, this means that small-scale clustering is naturally enhanced for these objects, causing a break in $\xi_{qq}(r)$ that occurs at larger radii for more luminous objects.

On the other hand, the luminosity dependence seen at $\gtrsim 2$ Mpc h^{-1} in the $z = 3$ bin is on such large scales that it can not be due to this effect. Instead this enhancement is likely to be a result of "geometrical bias," which is caused by the statistics of peaks within a Gaussian random field (*e.g.* Kaiser 1984; Bardeen *et al.* 1986; Mo & White 1996; Porciani *et al.* 1998). Note that on these scales the increase in $\xi_{qq}(r)$ is independent of distance, further pointing to this origin.

Similar trends are apparent in the comparison run. Again there is little luminosity dependence at $z \leq 2$ and $r \geq 1$ h^{-1} Mpc. Also as in the feedback case, strong luminosity dependence is detected in the two regimes that are least constrained observationally: small-scale ≤ 2 Mpc h^{-1} clustering, which is likely to be dominated by one-halo effects, and larger-scale high-redshift clustering, which is likely to be dominated by

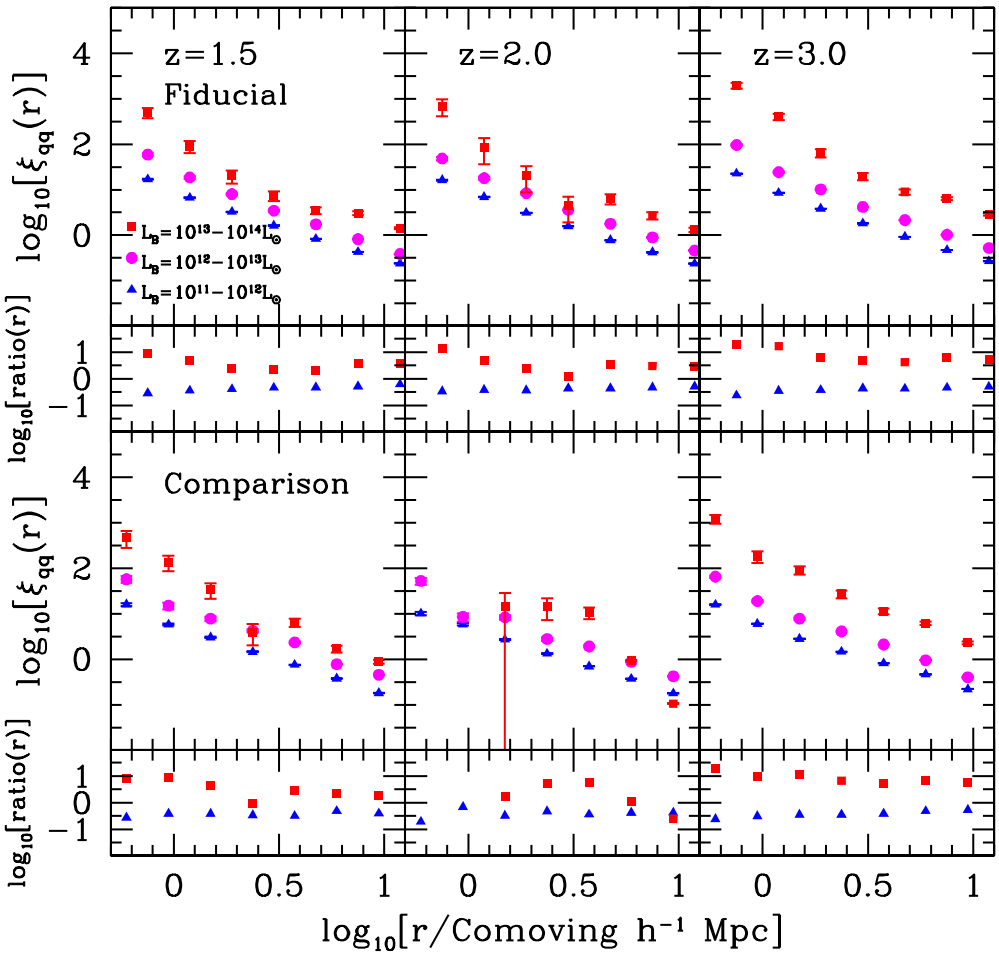

FIG. 3.— Luminosity and redshift dependence of the quasar auto-correlation function, $\xi_{qq}(r)$. The top row shows the results our AGN-feedback simulations, as calculated by partitioning quasars into bins with $L_B = 10^{11}-10^{12}L_{\odot,B}$, $L_B = 10^{12}-10^{13}L_{\odot,B}$, and $L_B = 10^{13}-10^{14}L_{\odot,B}$. In the second row we show the ratio of $\xi_{qq}(r)$ for $L_B = 10^{13}-10^{14}L_\odot$ quasars over $\xi_{qq}(r)$ for $L_B = 10^{12}-10^{13}L_\odot$ quasar (squares) and the ratio for $L_B = 10^{11}-10^{12}L_\odot$ quasars over $L_B = 10^{12}-10^{13}L_\odot$, quasars again from the AGN-feedback simulation. In the third row we show $\xi_{qq}(r)$ from our no feedback comparison simulation, with symbols as above, and the ratios of the correlation functions from this run are given the bottom row. As in Figure 2, from left to right each column shows the results from $z = 1.2-1.75$, $z = 1.75-2.25$, and $z = 2.25-4.0$, and all error bars are 1-sigma Poisson estimates.

geometric bias.

To quantify our results further we computed the bias of quasars as function of L and z as

$$b^2(L,z) = \frac{\sum_k w(r_k,L,z)\xi_{qq}(r_k,L,z)\xi_{DM}(r_k,z)^{-1}}{\sum_k w(r_k,L,z)}, \qquad (8)$$

where $\xi_{qq}(r_k,L,z)$ is the quasar auto-correlation function in a radial bin k as a function of luminosity and redshift, $\xi_{DM}(r,z)$ is the linear dark matter correlation function extrapolated to the redshift bin of interest, $w(r_k,L,z)$ is a weighting function that counts the number of pairs contributing to each value of $\xi_{qq}(r_k,L,z)$, and we average over the interval from r = 1.0 to 10 h^{-1} Mpc. Error bars are again computed from Poisson estimates. A selected list of the computed bias values is given in Table 1 and the full data-set is plotted in Figure 4, in which we have also compiled results from current surveys, extrapolating to the B-band with a spectral slope of $\alpha_\nu = -0.5$, (Wyithe & Loeb 2005; TSC06). Note however that these surveys do not necessarily estimate bias at exactly the same range of separations as we have used. In particular, this plot includes points from Porciani *et al.* (2004) and Porciani & Norberg (2006), measured at $\approx 2-20$ comoving h^{-1} Mpc, Adelberger & Steidel (2005), measured at ≤ 30 comoving h^{-1} Mpc, Croom *et al.* (2005), measured at $\approx 1-20$ comoving h^{-1} Mpc, and Myers *et al.* (2006; 2007a), measured from $\approx 1-100$ h^{-1} Mpc. Finally, for comparison purposes, we have also added a simple analytic estimate of the bias expected in the no feedback case, in which black hole mass can be directly related to the halo velocity dispersion and hence to the halo mass as in Wyithe & Loeb (2002). In this case,

$$b(L,z) = 1 + \delta_{0,c}^{-1}\left[\nu'^2 + b\nu'^{2(1-c)} - \frac{\nu'^{2c}/\sqrt{a}}{\nu'^{2c} + b(1-c)(1-c/2)}\right], \qquad (9)$$

where $a = 0.707$, $b = 0.5$, $c = 0.6$, $\delta_{0,c} = 1.69$, $\nu' = a^{1/2}\delta_{0,c}D(z)^{-1}\sigma^{-1}(M_{\rm halo})$, $D(z)$ is the linear growth factor, $\sigma(M_{\rm halo})$ is the $z = 0$ variance on the halo mass scale, $M_{\rm halo}$, corresponding to a given quasar luminosity (Sheth *et al.* 2001; see also Mo & White 1996; Jing 1999; Scannapieco & Barkana 2002), in the case in which gas accretion and dark matter collapse occur simultaneously, maintaining the cosmological ratio at all times.

Expressing our $\gtrsim 1$ h^{-1} Mpc results as a bias allows for easy quantification of the trends seen in Figure 3, as well as

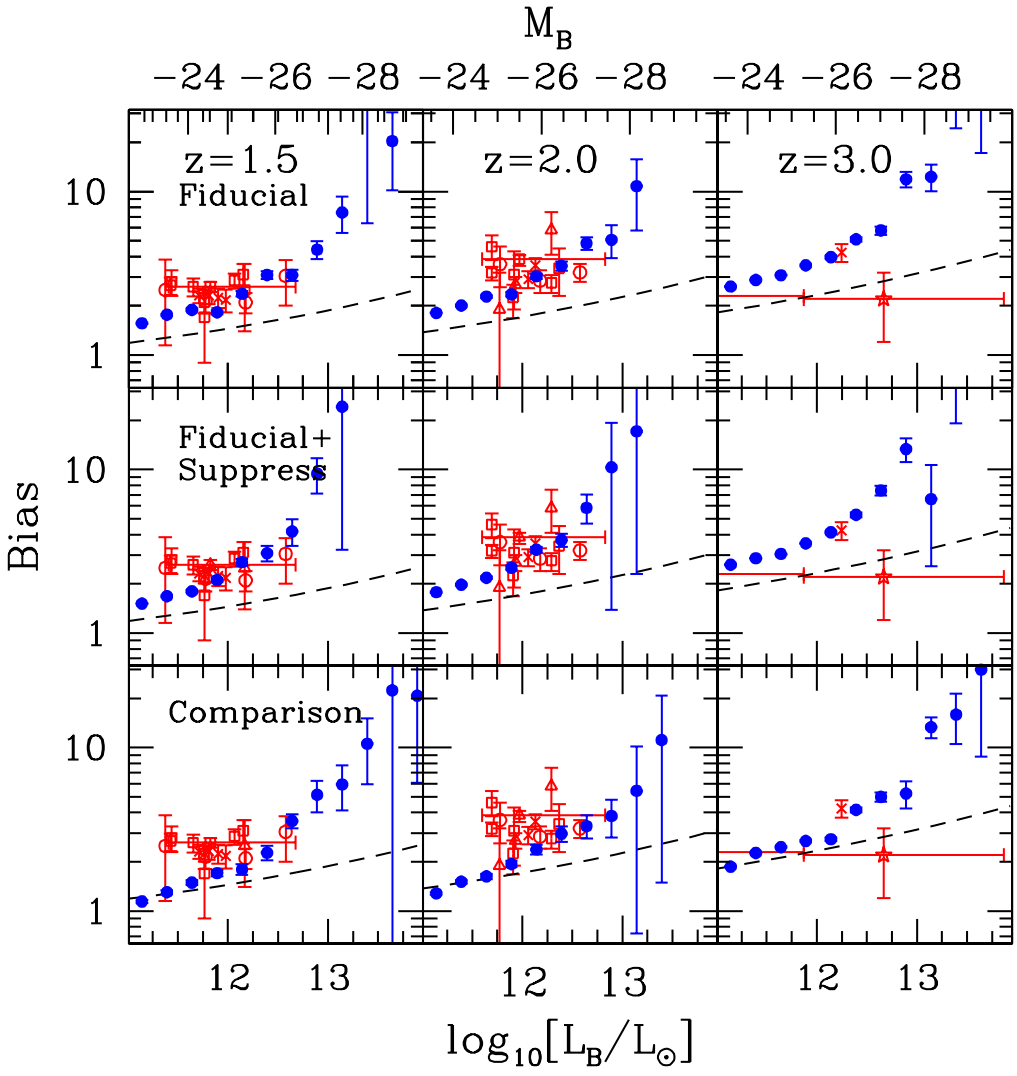

FIG. 4.— *Top:* Bias of quasars as a function of redshift and B-band luminosity. As in Figure 2, simulation results are given by the solid points with 1-sigma Poisson error bars, and the dashed line is the simple Sheth *et al.* (2001) estimate of the bias as described in the text. The open squares corresponds to the observational data points, which are taken from Porciani *et al.* (2004) and Porciani & Norberg (2006), open triangles; Croom *et al.* (2005), crosses; Adelberger & Steidel (2005), stars; and Myers *et al.* (2006; 2007a), squares. From top to bottom, the rows correspond to the fiducial run, the fiducial run with additional suppression, and the comparison run. Columns correspond to redshift bins as in Figures 2 and 3.

comparisons with observations. Focusing first on the AGN feedback results, we find that bias increases by no more than $\approx 50\%$ over the range of luminosities and redshifts probed by current surveys. The observational data indicate that current clustering bias measurements (Porcani *et al.* 2004; Adelberger & Steidel 2005; Croom *et al.* 2005; Porcani & Norberg 2006; Myers *et al.* 2006, 2007a) do not provide any significant statistical constraints above $\log_{10}(L_B/L_\odot) = 12.5$. Indeed, a sample large enough to detect luminosity dependence of bias with $\Delta b \simeq 1$ at a 3σ confidence level, given current detection limits (such as 2QZ), would require an all-sky measurement (Porcani & Norberg 2006). At $z = 3$, there is a suggestion in our simulations that bias changes significantly with luminosity above $\log(L_B) = 12$, but this regime is poorly-constrained observationally.

While this mismatch between the observed range of redshifts and luminosities and the regime in which we expect strong luminosity dependence appears initially to be somewhat of a conspiracy, it can be understood naturally as a consequence of our feedback modeling. As discussed in detail in Scannapieco *et al.* (2005) and TSC06, AGN outflows act to impose a maximum halo mass, above which gas is unable to cool efficiently, suppressing further generations of galaxies and quasars. Furthermore, as radiative cooling is proportional to the square of the gas density, cooling is much more efficient in dense, high-redshift structures than it is at lower redshifts. This means that the "quenching threshold" *i.e.* the mass at which AGN is shut down (Faber *et al.* 2007) should decrease with time, with the strongest AGN quenching galaxy formation even at high redshifts, but smaller smaller AGN quenching galaxy formation only at low redshifts. At the same time the hierarchical nature of dark-matter driven gravitational collapse means that the nonlinear mass scale *increases* with time, as ever-larger structures collapse and virialize.

This means that AGN are naturally divided into two regimes. At high redshift, the characteristic luminosity of active black holes brightens along with the nonlinear mass scale, while at low redshift, their characteristic luminosity fades along with the quenching threshold. The $z \approx 2$ peak of AGN activity then marks a distinct transition between hier-

TABLE 1
SELECTED CORRELATION LENGTHS AND BIASES FOR THE FIDUCIAL AND COMPARISON RUNS AS A FUNCTION OF REDSHIFT, LUMINOSITY, AND SELECTION BAND. OPTICALLY-SELECTED VALUES ARE GIVEN FIRST. A KEY OF 'F' CORRESPONDS TO THE FIDUCIAL RUN, WHILE 'C' TO THE COMPARISON RUN. BOLOMETRIC LUMINOSITIES ASSOCIATED WITH EACH BIN ARE GIVEN, ALONG WITH THE ASSOCIATED B-BAND LUMINOSITY (FOR THE OPTICAL CATALOG) AND HARD X-RAY LUMINOSITY (FOR THE X-RAY CATALOG). CORRELATION LENGTHS ARE QUOTED TO 2 SIGNIFICANT FIGURES WITHOUT ERRORS SINCE STATISTICAL ERRORS WILL BE SIGNIFICANTLY SMALLER THAN SYSTEMATIC ERRORS FROM THE BINNING PROCEDURE.

Run	z	$\log(L_{Bol}/L_\odot)$	$\log(L_B/L_\odot)$	M_B	L_X (erg s^{-1})	r_{cut} (h^{-1} Mpc)	r_0 (h^{-1} Mpc)	b
F	1.5	12.7	11.6	-24.3		10	5.2	1.9
F	1.5	12.7	11.6	-24.3		25	4.4	1.6
C	1.5	12.7	11.6	-24.3		10	4.1	1.5
F	2.0	12.7	11.6	-24.3		10	5.3	2.3
F	2.0	12.7	11.6	-24.3		25	4.6	2.0
C	2.0	12.7	11.6	-24.3		10	3.8	1.6
F	3.0	12.7	11.6	-24.3		10	5.4	3.1
F	3.0	12.7	11.6	-24.3		25	5.3	3.0
C	3.0	12.7	11.6	-24.3		10	4.3	2.5
F	1.5	13.2	12.1	-25.6		10	6.4	2.4
F	1.5	13.2	12.1	-25.6		25	6.3	2.2
C	1.5	13.2	12.1	-25.6		10	4.8	1.8
F	2.0	13.2	12.1	-25.6		10	7.2	3.0
F	2.0	13.2	12.1	-25.6		25	6.2	2.6
C	2.0	13.2	12.1	-25.6		10	5.6	2.4
F	3.0	13.2	12.1	-25.6		10	7.1	4.0
F	3.0	13.2	12.1	-25.6		25	7.4	4.0
C	3.0	13.2	12.1	-25.6		10	4.6	2.7
F	1.5	13.4	12.4	-26.2		10	7.8	3.1
F	1.5	13.4	12.4	-26.2		25	5.7	2.1
C	1.5	13.4	12.4	-26.2		10	6.3	2.3
F	2.0	13.4	12.4	-26.2		10	8.6	3.5
F	2.0	13.4	12.4	-26.2		25	6.9	2.9
C	2.0	13.4	12.4	-26.2		10	6.7	3.0
F	3.0	13.4	12.4	-26.2		10	9.1	5.1
F	3.0	13.4	12.4	-26.2		25	8.3	4.4
C	3.0	13.4	12.4	-26.2		10	7.5	4.1
F	1.75	10.0			3.2×10^{42}	10	3.9	1.6
C	1.75	10.0			3.2×10^{42}	10	3.1	1.2
F	1.75	11.3			3.2×10^{43}	10	3.6	1.5
C	1.75	11.3			3.2×10^{43}	10	3.2	1.3
F	3.0	11.3			3.2×10^{43}	10	3.3	2.0
C	3.0	11.3			3.2×10^{43}	10	3.2	1.8
F	1.75	12.6			3.2×10^{44}	10	5.2	2.1
C	1.75	12.6			3.2×10^{44}	10	4.5	1.7
F	3.0	12.6			3.2×10^{44}	10	5.5	3.1
C	3.0	12.6			3.2×10^{44}	10	4.5	2.5

archical and anti-hierarchical formation, which occurs when the quenching threshold drops below the nonlinear mass scale. Thus the majority of AGN formed at redshifts below the peak of AGN activity, meaning those that are easiest to observe and quantify, are naturally found in halos with masses well below the nonlinear mass scale. As can been seen from eq. (9), these low masses are very weakly biased, as b^2 is a strong function of ν' when $\nu' \gtrsim 1$, but almost a constant when $\nu' \lesssim 1$.

Another important feature of our feedback model is that it produces halo biases that are systematically offset from the no-feedback case. This is because feedback acts to slow accretion even before the quenching threshold is passed, meaning that each halo hosts a somewhat less massive black hole than it would have in the absence of feedback. Thus, for a fixed luminosity, each AGN is shifted to a somewhat more massive, and hence more clustered, dark matter halo, and the typical increase in bias over the no-feedback case is about 30%. At the faint end this corresponds to an increase over the analytic estimate of about a factor of ≈ 2. The quasars points from our simulation are also offset from the simple Sheth *et*

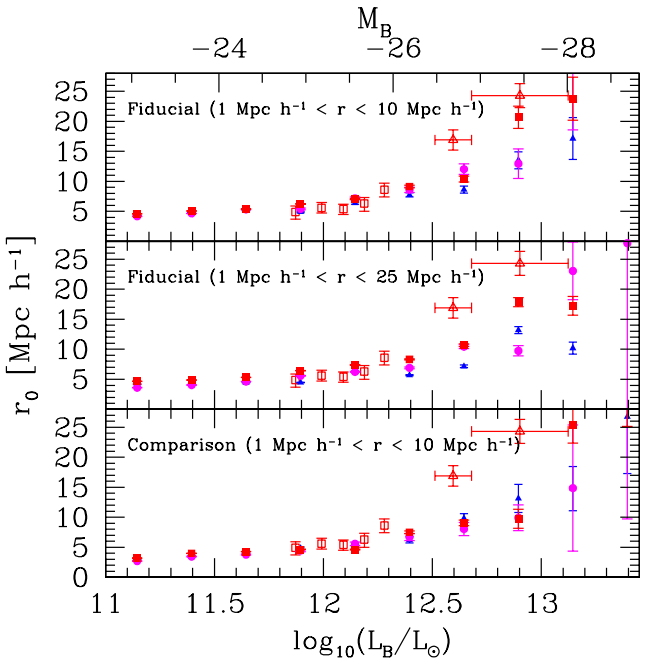

FIG. 5.— *Top:* Correlation length as a function of luminosity and redshift. The closed triangles, circles, and squares correspond to redshift bins $z = 1.5$, 2.0, and 3.0 respectively, with 1-sigma Poisson error bars. Open squares correspond to the $\gamma = 1.8$ fits of Porciani & Norberg (2006) to the 2QZ survey at redshifts $z = 0.93$, 1.19, 1.41, 1.60, 1.79, and 1.98, with the mean M_B being taken from Croom *et al.* (2005). Open triangles correspond to the Shen *et al.* (2007) SDSS data points for $2.9 < z < 3.5$ and $z > 3.5$, but are fitted for $\gamma = 2.0$ rather than 1.8 with i-band to B-band conversion taken from Hao *et al.* (2005).

al. (2005) estimates, again because gas accretion lags behind the dark matter collapse in the simulation.

It is important to note that post-processing our results to correct for the handful of very luminous, low-redshift AGN that result from inefficiency in shock heating in the simulation has very little effect on any of these trends, despite it leading to an almost perfect match of the luminosity function. As shown in the center row, removing these objects only impacts the $L_B \gtrsim 10^{13} L_\odot$ measurements in the lowest redshift bins, primarily increasing the already large error bars by further lowering the number density of these objects.

In the comparison run, on the other hand, the overall bias at each mass scale is somewhat lower than in either of the other two cases. Again this is because while gas accretion and cooling still take time, this time is much less than the $2-5$ Gyr Hubble times at these epochs, meaning that the relationship between black hole mass and halo mass is more in line with that expected purely from the dark matter distribution. Note that even in this run however, there is very little evolution in clustering over the *observed* range of luminosities. This is because even though no feedback is included, leading to a fair number of large and biased low-redshift AGN in the simulation, the lack of low redshift quasars in the data in the observations means these objects simply do not exist in nature, and thus can not be compared to our predictions. However, even in the absence of feedback, the significant cooling time associated with large objects means that gas accretion trails dark matter collapse. Thus means that quasars are found in higher-mass halos, and hence are more clustered, than one would expect in a simple model in which the gas accretion moves forward in lock-step with dark-matter collapse.

A second way to quantify our results is by using the correlation length, r_0, the scale at which $\xi_{qq} = 1$. If $\xi_{qq} \propto r^{-\gamma}$, this occurs at $r_0^\gamma = \xi_{qq}(r) r^\gamma$ for all choices of r. Thus we can compute r_0 by averaging this quantity over all radial bins r_k from 1 to 10 h^{-1} Mpc

$$r_0(L,z) = \left[\frac{\sum_k w(r_k,L,z)\xi_{qq}(r_k,L,z) r_k^\gamma}{\sum_k w(r_k,L,z)} \right]^{1/\gamma}, \qquad (10)$$

where we choose to set $\gamma = 1.8$ and ξ_{qq} is the quasar auto-correlation function as a function of luminosity L and redshift z. In Figure 5 we compare the results of this analysis with correlation length measurements from the 2QZ (range $1 < z < 2$) and SDSS (range $3 < z < 5$) surveys. A selected list of the computed correlation lengths is also given in Table 1.

The fiducial model, shown in the top panel, indicates that below $L_B \approx 10^{12} L_\odot$ there is little evolution in the correlation length either as a function of redshift or luminosity. The calculated correlation lengths are also in good agreement with the Croom *et al.* (2005) results. Above $L_B \approx 10^{12} L_\odot$, on the other hand, the variability of the correlation with luminosity is more evident, however even this seems to fall slightly short of the very large correlation length seen in the SDSS sample (although our quoted Poisson errors are smaller than the systematic errors from the binning procedure) . We note that our our highest redshift bin ($z = 2.25-4.0$) has a mean redshift less than that of the $z > 3.5$ SDSS bin, but the lower $2.9 < z < 3.5$ SDSS bin is comparable to our $z = 3$ predictions. The primary difference between results probably stems from the fact that the SDSS measurement considers pairs with separations from $4\,h^{-1}\mathrm{Mpc} < r < 150\,h^{-1}\mathrm{Mpc}$, which is a vastly larger range than can be probed with current simulations that retain high resolution in individual galaxies. In fact, it could be reasonably argued that a box of 1000 h^{-1} Mpc is necessary to study correlations on this scale. Additionally, considering correlations to such large radii is fraught with potential difficulties, since for redshifts $z \lesssim 1$ the galaxy-galaxy correlation function is expected to steepen for separations larger than $60 h^{-1}$ Mpc (see Springel, Frenk & White 2006). Were AGN/quasars to more closely trace the underlying dark matter auto-correlation function than the normal galaxy population at high redshift then the effective power law for the auto-correlation function would be expected to change by almost 50% as one moves from 5 h^{-1} Mpc to 20 h^{-1} Mpc (Porciani & Norberg 2006). Further, fitting steeper power laws will inherently tend to produce larger correlation lengths.

The steepening of the galaxy-galaxy correlation function is a product of the underlying bias of the galaxy population and the transition to the non-linear regime in the dark matter power spectrum, which occurs at $k > k_{nl} \simeq 0.1\,h\,\mathrm{Mpc}^{-1}$ at low redshift. This scale evolves comparatively slowly until $z \approx 1$, above which it begins to recede quickly, and by $z \simeq 3$ we find $k_{nl} \simeq 0.3\,h\,\mathrm{Mpc}^{-1}$. Semi-analytic models of the galaxy-galaxy correlation function are able to roughly preserve the location of this steepening point (see, *e.g.*, Springel *et al.* 2006) but do so through a rapidly increasing bias with redshift. If the bias of the AGN population does not increase sufficiently quickly with redshift then the clustering statistics will directly measure the underlying evolution in the non-linear scale. It is worth noting that current surveys at $z \approx 3$ definitely straddle the turnover in the dark matter correlation function. Thus the enhanced correlation seen in the SDSS might be related to a change in the radial position of the steepening of the correlation function with redshift. The precise details are dependent upon the redshift evolution of the bias of the AGN population

and, as we have indicated, our simulation box is too small to make any firm statements.

However, to study the dependence of our results on the much smaller distances we can probe, we recalculated eq. (10) using a range of separations from $r_k = 1\ h^{-1}$ Mpc to 25 h^{-1} Mpc. These values, shown in the second panel of Figure 5 demonstrate the correlation is decreased systematically when one includes more information from large separations. As discussed above in relation to Figure 3, the origin of these differences is most likely to be the excess contribution at small separations from the one-halo term, which becomes less important as moves from the shorter 10 h^{-1} Mpc cutoff to the longer 25 h^{-1} Mpc cutoff. Even this modest change in the outer cutoff can change the correlation lengths by as much as 40% (specifically in the z=1.5, $L_B = 12.4\,L_\odot$ bin) although the mean change is close to 15%.

Finally, in the lower panel, we show the results from our comparison simulation, which again displays similar trends as in the AGN feedback run, but with a lower level of clustering. For all models and separations it is difficult to draw conclusions about the redshift evolution of r_0. Indeed, our results support the idea of using correlation function evolution models that are roughly constant in comoving coordinates since we see little evolution in our comparison models (for example) at $\log_{10}(L_B/L_{\rm bol}) < 12.5$.

4. X-RAY SELECTED AGN

X-ray selection is widely believed to be an unbiased method for selecting AGN candidates, which is largely free from the obscuration and incompleteness issues that affect optical catalogs (*e.g.* Yang *et al.* 2006). While the exact nature of the optical versus X-ray light curves is the subject of debate (as summarized in Hopkins *et al.* 2008, and references therein), we examine the X-ray clustering of our catalog based on the same assumptions as our optical catalog. In this case the only differences between X-ray and optical selection come from bolometric correction factors, as even obscuration of optical systems should not impact the overall correlation unless obscuration is somehow a function of position. Additionally, so long as the average lifetime of the X-ray bright period is not longer than ≈ 1 Gyr, and hence peculiar velocities do not lead to systems moving an appreciable distance, our lifetime assumptions should not have a significant impact on clustering. Of course this is not true for the luminosity function, which is very sensitive to changes in lifetimes, and we have previously shown (TSC06) that the hard X-ray luminosity function calculated from our model reproduces the observations of Ueda *et al.* (2003).

To calculate the ratio of the intrinsic X-ray luminosity, L_X, to the bolometric luminosity, $L_{\rm Bol}$, within our simulation we use the following two-polynomial fits from Marconi *et al.* (2004),

$$\log[L_{\rm Bol}/L_X(2-10\,{\rm keV})] = 1.54+0.24\mathcal{L}+0.012\mathcal{L}^2+0.0015\mathcal{L}^3,$$
$$\log[L_{\rm Bol}/L_X(0.5-2\,{\rm keV})] = 1.65+0.22\mathcal{L}+0.012\mathcal{L}^2+0.0015\mathcal{L}^3, \quad (11)$$

where $\mathcal{L} = \log(L_{\rm Bol}) - 12$, and $L_{\rm Bol}$ is given in $L_\odot$. While a large number of estimates for bias and correlation lengths exist for $z \lesssim 1$ (*e.g.* Mullis *et al.* 2004; Gilli *et al.* 2005; Basilakos *et al.* 2004, 2005; Yang *et al.* 2006; Miyaji *et al.* 2007), the current observational data is too sparse at redshifts $z > 2$ to provide reliable statistics on redshift evolution. However, cross-correlating luminous blue galaxies and AGN allows a calculation of the bias of the AGN population at $z \simeq 3$ (Francke *et al.* 2008). We therefore calculate both the bias and correlation functions of our simulation, but split the catalog into only two redshift bins: $z = 1.2-2.0$, which we label as $z = 1.75$, and $z = 2.0-4.0$, which we label as $z = 3.0$. Within these bins we then calculate correlation functions and bias using the procedures outlined in section 3.2.

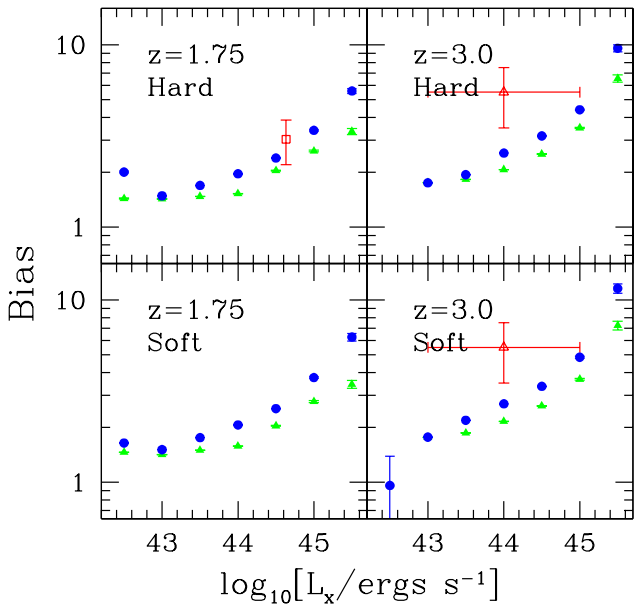

FIG. 6.— Bias of X-ray selected AGNs as a function of redshift and X-ray luminosity. The green triangles are from the comparison run, while the blue circles are from the fiducial feedback model, both with 1-sigma Poisson error bars. The open square data point on the $z = 1.75$ plot is from Yang *et al.* (2006), and corresponds to the bias for their $z = 1.5-3.0$ bin (no variance for the mean of the luminosity bin is given). The open triangle is from Francke *et al.* (2008) and gives their AGN bias calculated from the cross-correlation function of AGN and luminous blue galaxies at $z \simeq 3$. The error bars encapsulate their range in luminosity and the mean is likely rightward of the central value. While our fiducial run is in good agreement with the Yang *et al.* (2006) results, the $z \simeq 3$ result is clearly lower than Francke *et al.* (2008) data.

In Figure 6 we plot the bias of our catalog for both hard and soft bands in our two redshift bins. As for the optical catalog, we find that the simulation with quasar feedback has a higher bias than the comparison run. Again, the primary origin of this difference is that feedback forces AGN of a given luminosity into more massive, and thus more biased halos. The fiducial run hard X-ray data in the $z = 1.75$ bin are a good fit to the Yang *et al.* (2006) bias estimate from the CDF-N and CLASXS fields, which suggests that including feedback is necessary to bias halos sufficiently to match observations. Furthermore, comparison to the $z = 3$ bias estimates of Francke *et al.* (2008), calculated using the cross-correlation of AGN and luminous blue galaxies, shows that our numbers are low relative to these observations, and that AGN feedback is absolutely necessary to match these data. We achieve a marginal agreement if we take the low value of their error and also the higher end of the luminosity range, which is plausible since we plot the center of the range and the the mean of their bin is likely rightward of the central value. It is also worth noting that these results show that in our model the luminosity dependence begins to become more noticeable above 10^{43} erg s^{-1}.

Before examining our results further we mention that since the luminosities of the X-ray data we are considering are considerably lower than the equivalent optically-selected catalog, the observations we consider may well be probing different

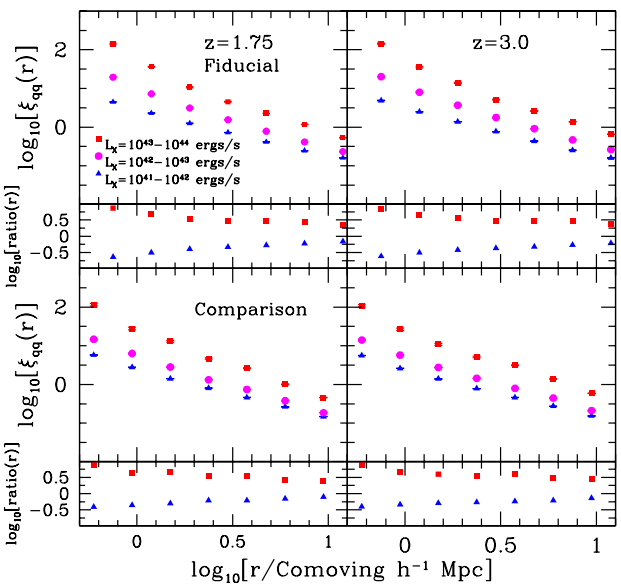

FIG. 7.— Correlation function of X-ray selected AGNs. We have divided the simulation into two redshift ranges, $z = 2.25-4.0$, which we label $z = 3$, and$z = 1.1-2.25$ which we label $z = 1.75$. We then bin into 3 decades of L_X, ranging from 10^{41} erg s^{-1}, to 10^{44} erg s^{-1}. The ratio of the 3.2×10^{43} erg s^{-1} to 3.2×10^{44} erg s^{-1} X-ray correlation functions increases by a factor of three in the one-halo regime, with a similar rise being observed in the optically selected catalogs. All error bars are 1-sigma Poisson estimates.

AGN fueling mechanisms as compared to our major merger model. In particular Hopkins & Hernquist (2006) have suggested that the limiting upper luminosity for where secular (*i.e.* Seyfert) effects or minor mergers become important is around $M_B \simeq -22$. This corresponds to an X-ray luminosity of 10^{44} erg s^{-1}, which is roughly in the middle of our considered X-ray luminosity range. However, since we compare directly to observations with mean luminosities above 10^{44} erg s^{-1} we can be reasonably confident that major mergers are the dominant physical process in these systems.

Both the fiducial and comparison runs correspond to the same bias at the faint end, ignoring the faintest bins at $z = 3$ which are at the limits of our resolution. However, the overall sensitivity to luminosity is higher for the fiducial run when examined over the entire range $L_X = [10^{43}, 10^{45.5}]$ erg s^{-1}, showing an increase in the bias of roughly a factor of 4 in the hard and soft X-ray bands at $z = 1.75$, and a factor of close to 6 in the $z = 3.0$ bin. Hints of this dependence are observed in the optical catalog over the range $\log(L_B) = [11.8, 12.6]$, although it is difficult to determine visually since the brighter bins have large error bars while the faint-end cutoff at $L_B = 10^{11.4}L_\odot$ does not probe as low in luminosity as the X-ray catalog. In the X-ray data, the ratio of the hard X-ray bias of the fiducial run to the comparison run is ≈ 1.6 for $L_X = 10^{45.6}$ erg s^{-1} at both $z = 1.75$ and $z = 3.0$ and the soft X-ray numbers are similar. The $L_X = 10^{45.5}$ erg s^{-1} bin also shows redshift evolution, with its bias decreasing by a factor of two from $z = 3$ to $z = 1.75$.

In Figure 7 we plot the correlation function of our X-ray selected AGN. While our estimates seem to be in good agreement with the data (the little studied $z = 3$ bin aside), the correlation lengths in this plot appear to be smaller than the observed data. Table 1 quantifies the correlation lengths extracted from the X-ray data using eq. (10), as well as selected correlation lengths and biases from throughout this paper. Observationally, Yang *et al.* (2006) give a combined CDF-N, CLASXS X-ray correlation length of $r_0 = 6.1^{+0.4}_{-1.0}h^{-1}$ Mpc, albeit with a shallow $\gamma = 1.47$ slope. Matching this correlation length at $z = 1.75$ with our luminosity binned data requires a mean luminosity greater than 3.2×10^{44} erg s^{-1}. However, just like the optical data these surveys have a much higher cutoff radius than our simulation. For example the CLASXS field discussed in Yang *et al.* (2006) considers pairs with separations up to 200 h^{-1} Mpc, well beyond beyond the radius at which the down-turn occurs in the galaxy-galaxy correlation function.

Recently, using luminosity binning, Plionis *et al.* (2008) have suggested that the wide variation in the correlation lengths of the CDF-S and CDF-N can be reconciled. They find evidence of strong evolution in clustering as a function of luminosity, with the correlation length in the hard X-ray band increasing from $\approx 6h^{-1}$ Mpc to $\approx 18h^{-1}$ Mpc, with a 0.7 dex increase in luminosity. A comparison to our X-ray correlation lengths in Table 1 shows that even our fiducial "light bulb" model cannot produce this level of luminosity dependence, nor can we produce the same underlying clustering. Thus although we do find a somewhat stronger trend for r_0 to increase with L_X than L_B, our results are at odds with Plionis et al. (2008) It is also worth noting that their quoted correlation length for the highest flux in the soft band of ≈ 30 h^{-1} Mpc is considerably larger than that quoted for the IRAC Shallow Cluster Survey (Brodwin *et al.* 2007), $r_0 = 19.14^{+5.65}_{-4.56}h^{-1}$ Mpc at $z = 0.97$. This implies that the comparatively low luminosity AGN (mean $L_X \approx 10^{43}$ erg s^{-1}) they sample are more strongly clustered at high redshift than $z = 1$ galaxy clusters. Ultimately more clustering data is needed to help understand the high redshift clustering of X-ray selected AGN, and we eagerly anticipate future all-sky surveys.

5. DISCUSSION

We have presented an analysis of our simulated quasar/AGN catalog, focusing on the dependence of real-space clustering on redshift, luminosity, and selection. Our model does not follow the detailed accretion history onto the central supermassive black hole (*e.g.* Hopkins *et al.* 2005a, 2005b, 2005c, 2006a, 2006b, 2007a), but rather takes a simple one-to-one correspondence between black hole mass and luminosity. Nonetheless we capture much of the essential physics in AGN formation and feedback. As a consistency check on our earlier work, we showed that a model that does not include feedback precisely follows the predicted luminosity function of the Wyithe & Loeb (2003) model, and thus fails badly at low redshift by overpredicting the observed numbers counts.

On the other hand, the qualitative luminosity function behavior is reproduced (TSC06) when feedback is included. Our clustering results are also in broad agreement with observed data, the main difference being somewhat less evolution with redshift than observed and somewhat smaller correlations lengths, although our bias values are in quantitative agreement within the observational errors. Furthermore for our "light bulb" model, the dependence of clustering with luminosity is weak at the luminosities probed by current surveys. Although the underlying relationship between quasar luminosity and black hole mass is likely to more complex than the simplified model assumed in this study (*e.g.* Ganguly *et al.* 2007), modeling these complexities dose not appear to be necessary to understanding current clustering measurements.

While the assumptions used in our calculations limit our analysis to scales above ≈ 0.5 Mpc h^{-1}, we are still able to

clearly observe one-halo effects, which occur within ≈ 2 Mpc h^{-1} for luminous AGN. Significantly, the luminosity dependence is more visible in this part of the correlation function as the two systems are embedded in a more highly biased halo. For example, the ratio of the 3.2×10^{43} erg s^{-1} to 3.2×10^{44} erg s^{-1} X-ray correlation functions increases by a factor of three in the one-halo regime. Deep quasar pair data would thus be extremely useful in helping to determine luminosity dependence in more detail.

However, we reemphasize that a straightforward comparison of current observations to our results, or those of any simulations, is not possible. While larger samples have made observational studies more robust, there still remain differences in fitted scales for correlation functions and the assumed slope of power-law fits. This is particularly important in the context of calculating correlation lengths, as departures from power-law fits occur both on small scales and large scales. On small scales the one-halo term produces a steepening in the effective index, while on large scales the transition from the non-linear to linear regime in the dark-matter power spectrum also produces a steepening of the effective index. We also note that redshift-space distortions (*e.g.* Croom et al. 2005; da Angela *et al.* 2005, 2008), can also produce departures from pure power-law behavior. Ultimately, the true power-law slope observed for the AGN/quasar population will depend on the underlying bias.

Given these facts and our modest outer radius of 25 h^{-1} Mpc, the fits we derive should be treated with due caution. For example, even for modest changes in the outer cutoff from 25 h^{-1} Mpc to 10 h^{-1} Mpc, our correlation lengths can increase by as much as 40%, although the mean change is close to 15%. The increase is directly associated with the one-halo contribution being given more weight in the case with the shorted outer cutoff, although we emphasize that all fits below 10 h^{-1} Mpc are within the non-linear scale at the epochs we are considering.

The redshift and luminosity dependence of large-scale clustering is a product of two competing effects: growth of the non-linear mass scale with time and a decrease in the mass scale of the quenching threshold that limits the supply of fuel to AGN. This quenching is primarily a function of the mean density of the gas, which controls its cooling rate. Thus at high redshifts, when radiative cooling is extremely efficient, feedback is weak, and the luminosity of black holes grows along with the nonlinear mass scale. However, once feedback is able to heat gas to a cooling time longer than the Hubble time, the fuel supply for luminous AGN is quenched, and this quenching become more efficient as the universe expands. The net result is a peak in AGN activity at redshift $z \approx 2$: AGN formed after this redshift correspond to low-mass, low-bias halos and show a weak luminosity dependence, and AGN formed before this redshift correspond to a wide range of biases and show an appreciable luminosity dependence. Thus the clustering behavior of AGN is a direct result both of the evolution of dark matter halos and the physics of AGN feedback.

We are grateful to Michael Strauss for useful comments and Phil Hopkins for making his compilation of quasar luminosity function data freely available. We also thank an anonymous referee for suggestions that improved the content of the paper. Figure 1 was produced using the "Splotch" package (`http://dipastro.pd.astro.it/~cosmo/Splotch/`). Computing was performed at WestGrid (under a RAC grant), ACEnet and on the *Computational Astrophysics Laboratory* at Saint Mary's University. R.J.T. acknowledges funding via a Discovery Grant from NSERC, the Canada Research Chairs program and the Canada Foundation for Innovation. M.R. was funded by an NSERC USRA. HMPC acknowledges funding from NSERC and the support of the Canadian Institute for Advanced Research.

REFERENCES

Adelberger, K. L., & Steidel, C. C. 2005, ApJ, 627, L1
Babul, A., Balogh, M. L., Lewis, G. F., & Poole, G.B. 2002, MNRAS, 330, 329
Bardeen, J. M., Bond, J. R., Kaiser, N., & Szalay, A. S. 1986, ApJ, 304, 15
Basilikos, S., *et al.* 2004, ApJ, 607, L79
Basilikos, S., *et al.* 2005, MNRAS, 356, 183
Begelman, M. C., & Cioffi, D. F. 1989, ApJ, 345, L21
Berlind, A. A., & Weinberg, D. H. 2002, ApJ,575, 587
Brighenti, F., & Mathews, W. G. 2001, ApJ, 553, 103
Brodwin, M., Gonzalez, A. H., Moustakas, L. A., Eisenhardt, P. R., Stanford, S. A., Stern, D., & Brown, M. J. I. 2007, ApJ, 671, L93
Bullock, J. S., Wechsler, R., H., & Somerville, R. S. 2002, MNRAS, 329, 246
Cattaneo, A., Dekel, A., Devriendt, J., Guiderdoni, B., & Blaziot, J. 2006, MNRAS, 370, 165
Cattaneo, A. *et al.* 2007, MNRAS, 377, 63
Chartas, G., Brandt. W. N., Gallagher, S.C., & Proga, D. 2007, AJ, 113, 1849
Croom, S. M., & Shanks, T. 1996, MNRAS, 281, 893
Croom, S. M., *et al.* 2004, MNRAS, 349, 1397
Croom, S. M., *et al.* 2005, MNRAS, 356, 415
Croton, D. *et al.* 2006, MNRAS, 365, 11
Couchman, H. M. P. 1991, ApJ, 386, L23
Cox, T. J., Di Matteo, T., Hernquist, L., Hopkins, P. F., Robertson, B., & Springel, V. 2006a, ApJ, 643, 69
Cox T. J., *et al.* 2006b, ApJ, 650, 791
da Angela, J. *et al.* 2005, MNRAS, 360, 1040
da Angela, J. *et al.* 2008, MNRAS, 360, 1040
Di Matteo, T., Springel, V., & Hernquist, L. 2005, Nature, 433, 604
Di Matteo, T., Colberg, J., Springel, V., Hernquist, L., & Sijacki, D. 2008, ApJ, 676, 33
Eisenstein, D., & Hu, W. 1999, ApJ, 511, 5
Elvis, M. *et al.* 1994, ApJS, 94,1
Erb, D. K., 2008, 674, 151
Faber, S. M. *et al.* 2007, ApJ, 665, 265
Ferrarese, L., & Merritt, D. 2000, ApJ, 539, L9
Ferrarese, L. 2002, ApJ, 578, 90
Francke, H., *et al.* 2008, ApJ, 673, L13
Furlanetto, S., & Loeb, A. 2001, ApJ, 556, 619
Ganguly, R. *et al.* 20007, ApJ, 665, 990
Gawiser, E., *et al.* 2006, ApJS, 162, 1
Gilli, R., *et al.* 2003, ApJ, 592, 721
Gilli, R., *et al.* 2005, A&A, 462, 865
Gingold, R. A., & Monaghan, J. J. 1977, MNRAS, 181, 375
Granato, G. L., *et al.* 2004, ApJ, 600, 580
Hao, L., *et al.* 2005, AJ, 129, 1795
Helly, J. C., Cole, S., Frenk, C. S., Baugh, C. M., Benson, A., Lacey, C., & Pearce, F. R. 2003, MNRAS, 338, 913
Hennawi, J. F., *et al.* 2006, AJ, 131, 1
Hopkins, P. F., & Hernquist, L. 2006, ApJS, 166, 1
Hopkins, P.F., Hernquist, L., Cox, T. J., Di Matteo, T., Martini, P., Robertson, B., & Springel, V. 2005a, ApJ, 630, 705
Hopkins, P.F., Hernquist, L., Cox, T. J., Di Matteo, T., Robertson, B., & Springel, V. 2005b, ApJ, 630, 716
Hopkins, P.F., Hernquist, L., Cox, T. J., Di Matteo, T., Robertson, B., & Springel, V. 2005c, ApJ, 632, 81
Hopkins, P.F., Hernquist, L., Cox, T. J., Di Matteo, T., Robertson, B., & Springel, V. 2006a, ApJS, 163, 1
Hopkins, P. F., Somerville, R. S., Hernquist, L., Cox, T. J., Robertson, B., & Li, Y. 2006b, ApJ, 652, 864
Hopkins, P. R., Lidz, A., Hernquist, L., Coil, A., L., Myers, A. D., Cox, T., J., & Spergel, D. N. 2007a, ApJ, 662, 110
Hopkins, P. F., Richards, G. T., & Hernquist, L., 2007b, 654, 731
Hopkins, P.F., Hernquist, L., Cox, T. J., & Kereš, D. 2008, ApJS, 175,356

Iovino, A., & Schaver, P. A. 1988, ApJ, 330, L13
Jing, Y. P. 1999, ApJ, 515, L45
Kaiser, N. 1984, ApJ, 284, L9
Kauffmann, G., & Haehnelt, M. 2000, MNRAS, 311, 576
Kravtsov, A. V., & Yepes, G. 2000, MNRAS, 318, 227
Kundic, T. 1997, ApJ, 482, 631
La Franca, F., Andreani, P., & Christiani, S., 1998, ApJ, 497, 529
Lidz, A., Hopkins, P. F., Cox, T. J., Hernquist, L., & Robertson, B. 2006, ApJ, 641, 41
Lucy, L. B. 1977, AJ, 82, 1013
Nagamine, K., Cen, R., Hernquist, L., Ostriker, J. P., & Springel, V. 2005, ApJ, 627, 608
Noeske, K. G. *et al.* 2007, ApJ, 660, L43
Marconi, A., Risaliti, G., Gilli, R., Hunt, L. K., Maiolino, R., & Salvati, M. 2004, MNRAS, 351, 169
Magliocchetti, M., & Porciani, C. 2003, MNRAS, 346, 186
Merritt, D., & Ferrarese, L. 2001, ApJ, 547, 140
Miyaji, T., *et al.* 2007, ApJS, 172, 396
Mo, H. J., & White, S. D. M. 1996, MNRAS, 282, 347
Mullis, C. R., *et al.* 2004, ApJ, 617, 192
Mushotsky, R. 2004, in Supermassive Black Holes in the Distant Universe, ed. A. J. Barger (Dordrecht: Kluwer), 53
Myers, A. D., *et al.* 2006, ApJ, 638, 622
Myers, A. D., Brunner, R. J., Nichol, R. C., Richards, G. T., Schneider, D. P., & Bahcall, N. A. 2007a, ApJ, 658, 85
Myers, A. D., Brunner, R. J., Nichol, R. C., Richards, G. T., Schneider, D. P., & Bahcall, N. A. 2007b, ApJ, 658, 99
Nath, B. B., & Roychowdhury, S. 2002, MNRAS, 333, 145
Okamoto, T., Nemmen, R. S., & Bower, R. G. 2008, MNRAS, 385, 161
Plionis, M., Rovilos, M., Basilikos, S., Georgantopoulos, I., & Bauer, F. 2008, ApJ, 674, L5
Porciani, C., Matarrese, S., Lucchin, F., & Catelan, P. 1998, MNRAS, 298, 1097
Porciani, C., Magliocchetti, M., & Norberg, P. 2004, MNRAS, 335, 1010
Porciani, C., & Norberg, P. 2006, MNRAS, 371, 1824
Proga, D., Ostriker, J. P., & Kurosawa, R. 2008, ApJ, 676, 101
Richards, G. T., *et al.* 2005, MNRAS, 360, 839
Richards, G. T., *et al.* 2006, AJ, 131, 2766
Robertson, B. *et al.* 2006a, ApJ, 641, 21
Robertson, B. *et al.* 2006b, ApJ, 641, 90
Serber, W., Bahcall, N., Menard, B., & Richards, G. 2006, ApJ, 643, 68
Scannapieco, E., & Barkana, R. 2002, ApJ, 571, 585
Scannapieco, E., & Oh, S. P. 2004, ApJ, 608, 62 (SO04)
Scannapieco, E., Silk, J., & Bouwens, R. 2005, ApJ, 635, L13
Scannapieco, E., Thacker, R. J., & Couchman, H. M. P. 2008, ApJ, in press
Scoccimarro, R. 1998, MNRAS, 299, 1097
Shen, Y. *et al.* 2007, AJ, 133, 2222
Sheth, R. M., Mo, H. J., & Tormen, G. 2001, MNRAS, 308, 199
Siana, B., *et al.* 2008, ApJ, 675, 49
Sijacki, D., Springel, V., Di Matteo, T., & Hernquist, L. 2007, MNRAS, 380, 877
Spergel, D. N., *et al.* 2003, ApJS, 148, 175
Springel, V., Di Matteo, T., & Hernquist, L. 2005a, ApJ, 620, L79
Springel, V., Di Matteo, T., & Hernquist, L. 2005b, MNRAS, 361, 776
Springel, V., Frenk, C., & White, S. D. M. 2006, Nature, 440, 1137
Szapudi, I., Quinn, T., Stadel, J., & Lake, G. 1999, ApJ , 517, 54
Thacker, R. J., Scannapieco, E., & Couchman, H. M. P. 2006, ApJ, 653, 86 (TSC06)
Thacker, R. J. & Couchman, H. M. P. 2006, Computer Physics Communications, 174, 540
Tornatore, L., Borgani, S., Matteuci, F., Recchi, S., & Tozzi, P. 2004, MNRAS, 349, L19
Tozzi, P., Scharf C., & Norman, C. 2000, ApJ, 542, 106
Tremaine, S., *et al.* 2002, ApJ, 574, 740
Ueda, Y., Akiyama, M., Ohta, K., & Miyaji, T. 2003, ApJ, 598, 886
van den Bosch, F. C., Yang, X., & Mo, H. J. 2003, MNRAS, 340, 771
Wolf, C., Wisotzki, L., Borch, A., Dye, S., Kleinheinrich, M., & Meisenheimer, K. 2003, A&A, 408, 499
Woo, J.-H., Treu, T., Malkan, M. A., Blandford, R., arXiv:0804.0235
Wyithe, J. S. B., & Loeb, A. 2002, ApJ, 581, 886
Wyithe, J. S. B., & Loeb, A. 2003, ApJ, 595, 614
Wyithe, J. S. B., & Loeb, A. 2005, ApJ, 621, 95
Yamada, M., Sugiyama, N., & Silk, J. 1999, ApJ, 522, 66
Yang, Y., *et al.* 2006, ApJ, 645, 68